Editors' Suggestion

Radiative Thermal Memristor

Jose Ordonez-Miranda,[1,*] Younès Ezzahri,[1,†] Jose A. Tiburcio-Moreno,[2] Karl Joulain,[1] and Jérémie Drevillon[1]
[1]Institut Pprime, CNRS, Université de Poitiers, ISAE-ENSMA, F-86962 Futuroscope Chasseneuil, France
[2]Universidad Nacional Jorge Basadre Grohmann, Facultad de Ciencias, Avenida Miraflores s/n, Ciudad Universitaria, 23003 Tacna, Perú

(Received 4 March 2019; revised manuscript received 14 May 2019; published 12 July 2019)

Based on the thermal hysteresis of a phase change material exchanging radiative heat with a phase invariable one, we propose a radiative thermal memristor characterized by a Lissajous curve between their exchanged heat flux and temperature difference periodically modulated in time. For a memristor with terminals of VO_2 and a blackbody, it is shown that (i) the temperature variations of its memristance follow a closed loop determined by the thermal hysteresis width of VO_2, and (ii) the thermal memristance on-off ratio is determined by the contrast of VO_2 emissivities for its insulating and metallic phases and is equal to 3.6. The analogy of the proposed memristor to its electrical counterpart makes it promising to lay the foundations of the thermal computing with photons.

DOI: 10.1103/PhysRevLett.123.025901

The last 15 years have witnessed the emergence of the new research area *thermotronics* devoted to the development of thermal analogues of the fundamental electronic components, by means of the heat transport via phonons, electrons, and photons [1–12]. Several conceptual devices, such as thermal rectifiers or diodes [13–19], thermal transistors [20–26], thermal logical gates [27] and thermal memories [28] have been proposed, and the working principles of some of them have experimentally been proven [29–31], which makes it possible to process information through heat currents.

The electrical memristor, a two-terminal device relating electrical charge with magnetic flux in electronic circuits, has recently attracted enormous interest due to its tremendous and revolutionary potential in microelectronics, informatics, spintronics, and neuromorphic networks [9,32]. Based on symmetry arguments, Chua [33] first conceived this device in 1971 as the fourth fundamental electronic component besides the resistor, capacitor, and inductor. Almost 40 years later, Strukov *et al.* [34] developed the physical model for describing the hysteretic current-voltage behavior that characterizes an electrical memristor and showed that its realization can be achieved with doped metal-oxide semiconductors.

Despite the vast research on and development of the electrical memristor [32], its thermal counterpart has received little attention. Based on the asymmetric temperature response of the thermal conductivity of VO_2 during its heating and cooling, Ben-Abdallah [35] proposed a conductive thermal memristor whose Lissajous curve between the heat flux and the temperature difference of its terminals was recently reported by Yang *et al.* [36]. The operation of this promising memristor is driven by the hysteretic metal-insulator transition of VO_2, which is one of the most investigated phase change materials (PCMs) due to its ability to change its thermal, optical, and electrical properties in a narrow interval of temperatures near room temperature [37–41]. The performance of the conductive memristor is, however, limited by the inevitable presence of interface thermal resistances and the speeds of the involved phonons and electrons, which are typically 3 orders of magnitude smaller than that of photons. These limitations could thus be overcome by a radiative memristor with contactless terminals.

The purpose of this Letter is to demonstrate the proof of principle of a radiative thermal memristor, an analogue of the electrical memristor defined by the functional relation $\Delta T = M(x,q)q$ between the temperature difference (ΔT) and heat flux q of a system with a generalized thermal resistance $M(x,q)$ determined by q and a state variable x driving the internal state of the system [33,34]. The $q-\Delta T$ characteristic curve of this memristive system is generally a Lissajous figure crossing the origin ($q=0$ for $\Delta T=0$), which distinguishes it from an arbitrary dynamical system, such as the case of an electrical memristor [34].

Let us consider a PCM exchanging heat by far-field thermal radiation with a non-PCM, due to their temperature difference $\Delta T(t)$ periodically modulated in time t, as shown in Fig. 1. The emissivity ε_1 of the PCM depends on its temperature $T_0+\Delta T(t)$, while the one ε_2 of the non-PCM is considered to be independent of its corresponding steady-state temperature T_0, as in the case of SiO_2 and SiC, for $T_0 < 600$ K [42]. In order to ensure the thermalization of the PCM, we consider the fact that the modulation period τ of $\Delta T(t)$ is much longer than its thermalization time (the time required to reach the thermal equilibrium between its electrons and phonons), which typically ranges from a few to 100 μs, for the case of VO_2 [37,43] used in this work.

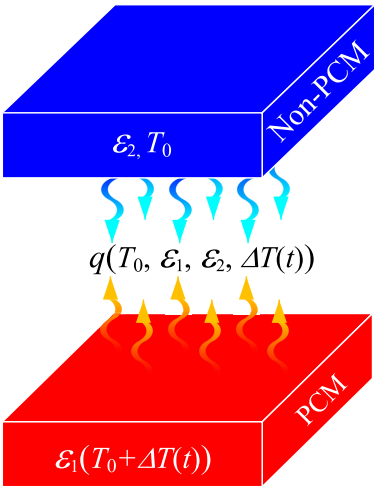

FIG. 1. Scheme of a radiative thermal memristor: a PCM exchanging radiative heat with a non-PCM through a vacuum gap due to their temperature difference $\Delta T(t)$ periodically modulated in time t.

This condition is good enough to guarantee that the heating frequency ($\tau^{-1} \lesssim 1$ MHz) is much smaller than the spectral frequencies of the photons emitted by the two materials, which are on the order of Terahertz, for temperatures near room temperature [44]. Under this quasisteady state, the far-field heat flux q exchanged by the two plates is given by the Stefan-Boltzmann law, as follows [44]:

$$q = \sigma\varepsilon[T_0 + \Delta T(t)]\{[T_0 + \Delta T(t)]^4 - T_0^4\}, \qquad (1)$$

where σ is the Stefan-Boltzmann constant and the effective emissivity $\varepsilon = (\varepsilon_1^{-1} + \varepsilon_2^{-1} - 1)^{-1}$ is determined by the emissivities of the PCM and non-PCM [44]. For the sake of simplicity, we will consider this non-PCM to be a blackbody ($\varepsilon_2 = 1$), which reduces the effective emissivity to that of the PCM ($\varepsilon = \varepsilon_1$).

We consider the fact that the emissivity ε of the PCM changes for temperatures within its phase transition, such that its value (ε_h) during the heating process is different than that (ε_c) for the cooling one, at a given temperature T, as in the case for VO_2 [37,45–47]. This thermal hysteresis of the PCM emissivity is driven by correlated atomic interactions and establishes the fact that ε is given by

$$\varepsilon(T) = \varepsilon_h(T)\delta(T\uparrow) + \varepsilon_c(T)\delta(T\downarrow), \qquad (2)$$

where $\delta(T\uparrow)$ and $\delta(T\downarrow)$ take the value of unity as the PCM temperature raises and lowers, respectively; otherwise they reduce to zero. For VO_2, the emissivities ε_h and ε_c can be well described by the following model [48]:

$$\varepsilon_n(T) = \varepsilon_i + \frac{\varepsilon_m - \varepsilon_i}{1 + e^{-\beta(T-T_{0n})}}, \qquad (3)$$

where $\varepsilon_i = 0.79$ and $\varepsilon_m = 0.22$ are the emissivities of VO_2 in its insulating and metallic phases, respectively,

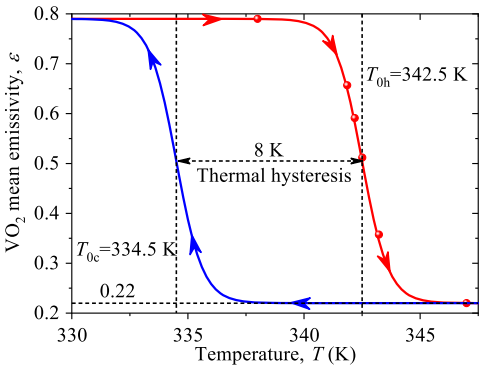

FIG. 2. Mean emissivity of VO_2 for its heating and cooling processes. The dots stand for experimental data [40,41,48], while the lines represent the predictions of Eq. (3).

$T_{0h} = 342.5$ K and $T_{0c} = 334.5$ K are its respective transition temperatures for the heating ($n = h$) and cooling ($n = c$) processes, and $\beta = 1.57$ K^{-1}. Equations (2) and (3) thus take into account the VO_2 thermal hysteresis of $T_{0h} - T_{0c} = 8$ K experimentally observed by Qazilbash *et al.* [40], and they indicate that the VO_2 emissivity is bounded between its values for the metallic and insulating phases ($\varepsilon_m \le \varepsilon_1 \le \varepsilon_i$), as shown in Fig. 2. Note that at low temperatures ($T < 332$ K), VO_2 behaves as an insulator with high emissivity, while for high temperatures ($T > 345$ K), it becomes a metal with low emissivity such that its emissivity changes a factor of $\varepsilon_i/\varepsilon_m = 3.6$ across its phase transition. This significant emissivity contrast in a relatively small temperature interval allows us to enhance (reduce) the radiative heat flux with VO_2 in its insulating (metallic) phase, as established by Eq. (1).

According to Eq. (1), the emissivity variations of VO_2 between its insulating and metallic phases along with its thermal hysteresis generate a closed loop for the evolution of heat flux q, as the temperature difference ΔT periodically changes through time. This loop unfolds in two coupled loops (the Lissajous curve) by properly modulating ΔT through positive and negative values, as shown below. The effective thermal resistance $\Delta T/q$ of the system (Fig. 1) will thus depend on ΔT and its sign (heating or cooling), which represents the history of the input temperature difference. This thermal memory effect is analogous to that of an electrical memristor characterized by a Lissajous I-V curve that induces the dependence of its electrical resistance on the input voltage difference and its polarity [34]. The radiative system shown in Fig. 1 can thus play the role of a thermal memory resistor (thermal memristor) with a memory resistance (memristance) $M = \Delta T/q$ given by Eq. (1), as follows:

$$M^{-1} = \sigma\varepsilon(T_0 + \Delta T)(2T_0 + \Delta T)[(T_0 + \Delta T)^2 + T_0^2]. \qquad (4)$$

Taking into account the fact that the PCM temperature $T_0 + \Delta T$ determining the values of M also drives the appearance of

metallic (insulating) domains in an insulating (a metallic) matrix during the heating (cooling) process [37], the memristance can also be described in terms of the volume fraction of these microscopic domains [40,41]. For instance, the volume fraction f_h of the metallic domains appearing during the heating of VO_2 at temperature T is given by [37] $f_h(T) = (-T/U)W_0\{-(U/2T)\exp(-U/T)\mathrm{erfc}[2\beta(T_{0h} - T)/5]\}$, where $W_0(\cdot)$ is the main branch of the Lambert W function, $\mathrm{erfc}(\cdot)$ is the complementary error function, and U is the activation energy (in units of kelvin) of the metallic domains. Taking into account the facts that $U \ll T$ [37] for all temperatures within the VO_2 phase transition and that $W_0(x \ll 1) \approx x$, this latter relation reduces to $f_h(T) \approx 0.5\mathrm{erfc}[2\beta(T_{0h} - T)/5] \approx \{1 + \exp[-\beta(T - T_{0h})]\}^{-1}$, which, in combination with Eq. (3), yields

$$f_h(T) = \frac{\varepsilon_i - \varepsilon_h(T)}{\varepsilon_i - \varepsilon_m}. \tag{5}$$

Equation (5) thus relates the microstructural parameter f_h of VO_2 with its emissivity ε_h for the heating process. For the cooling process, on the other hand, one can show that the known volume fraction f_c [37] of the metallic matrix of VO_2 containing its insulating domains also reduces to Eq. (5) provided that $U \ll T$ and that the subindex h is replaced by c. The common dependence of f_n, ε_n, and M on the PCM temperature $T_0 + \Delta T$ allows us therefore to consider the ensemble of Eqs. (2)–(5) a system of parametric equations for the evolution of the thermal memristance $M(f)$ with the volume fraction $f = f_h\delta(T\uparrow) + f_c\delta(T\downarrow)$ describing the degree of metallization of VO_2 across its phase transition. This control of the thermal memristance by the state variable f reinforces its analogy with the electrical memristance, whose values are driven by the electrical charge [34], which is a state variable in electricity.

The heat flux and memristance are now numerically analyzed for a thermal memristor made up of a VO_2 plate exchanging radiative heat with a blackbody. To capitalize on the thermal hysteresis of the VO_2 emissivity, the reference temperature $T_0 = (T_{0h} + T_{0c})/2 = 338.5$ K is set as the average of the insulating-to-metal and metal-to-insulating transition temperatures. Furthermore, we consider a temperature difference $\Delta T(t) = \theta\sin(2\pi t/\tau)$ varying sinusoidally with time, in a similar way as the electrical memristor, which is usually excited with an alternating voltage difference [33,34]. The amplitude θ is chosen large enough ($\theta \geq T_{0h} - T_{0c} = 8$ K) to ensure that VO_2 completes its hysteresis loop after one period τ. In practice, this periodic oscillation of the PCM temperature can be set with a Peltier cell [49], while the non-PCM is kept at constant temperature with a second Peltier cell. These cells typically operate with a resolution better than 0.1 K [50] and modulation frequencies from 0.1 up to 100 Hz, which are much smaller than the infrared ones driving the thermal radiation at temperatures around T_0. This is the reason why the oscillating temperature of the PCM is not expected to significantly alter the equilibrium state of the emitted photons in the radiative thermal memristor shown in Fig. 1.

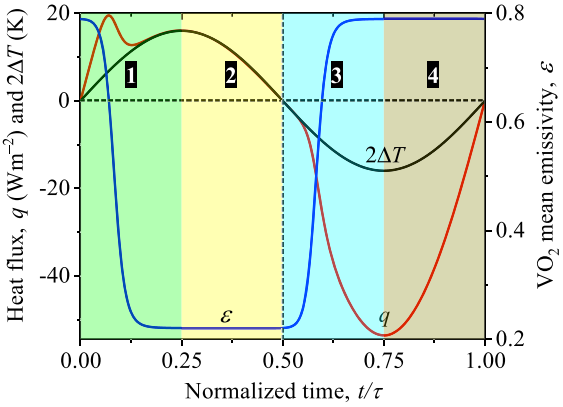

FIG. 3. Time evolution of the heat flux, temperature difference, and VO_2 emissivity driving the thermal radiation in the memristor shown in Fig. 1. The colored zones 1 and 3 stand for phase transitions, while zones 2 and 4 represent no phase changes. Calculations were done for $\theta = 8$ K.

Figure 3 shows the heat flux q, temperature difference ΔT, and VO_2 emissivity ε driving the thermal radiation in the thermal memristor as functions of time. Note that ε exhibits four different behaviors within one period τ. In case 1 ($0 \leq t/\tau < 0.25$), ε drastically reduces due to the insulator-to-metal transition of VO_2 as ΔT increases. An additional increase and then decrease of ΔT keeps the VO_2 in its metallic phase with constant and low emissivity, as revealed by case 2 ($0.25 \leq t/\tau < 0.50$). In case 3 ($0.50 \leq t/\tau < 0.75$), ΔT continues reducing and triggers the metal-to-insulator transition of VO_2 characterized by the significant increase of ε, as shown in Fig. 2. The subsequent variations of ΔT maintain the VO_2 in its insulating phase with constant and high emissivity, as displayed by case 4 ($0.75 \leq t/\tau < 1$). The combined time variations of ΔT and ε for cases 1 and 3 induce a heat flux with a strong nonlinear dependence on the temperature difference, despite the fact that $\Delta T \ll T_0 = 338.5$ K. For cases 2 and 4, on the other hand, ε takes constant values and $q \propto \Delta T$, as shown in Fig. 3 by the occurrence of the maximum and minimum values q and ΔT at the same time, and it is established by Eq. (1) for $\Delta T \ll T_0$. It is thus clear that the sharp variations of the heat flux with respect to those of the temperature difference are generated by the phase transitions of VO_2.

The Lissajous $q - \Delta T$ curve of the proposed thermal memristor is shown in Fig. 4. The cycle direction is indicated by the arrows associated with the four behaviors illustrated in Fig. 3. The straight lines in cases 2 and 4 confirm the proportionality ($q = G\Delta T$) between the heat flux and the temperature difference due to the absence of VO_2 phase transitions. The slope $G = M^{-1}$ is the thermal

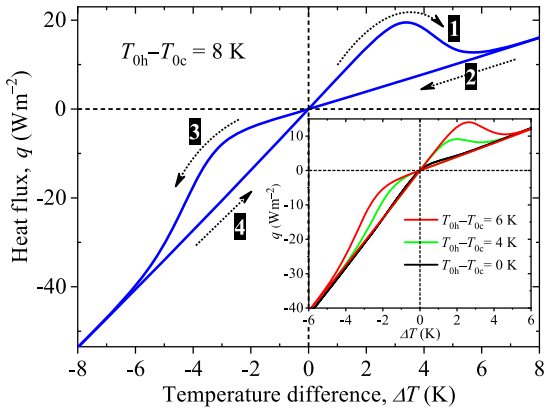

FIG. 4. Lissajous $q-\Delta T$ curve characterizing the thermal memristor. Regimes 1, 2, 3, and 4 correspond to the four characteristic zones highlighted in Fig. 3. Calculations were done for $\theta = 8$ K and different hysteresis widths $T_{0h}-T_{0c}$.

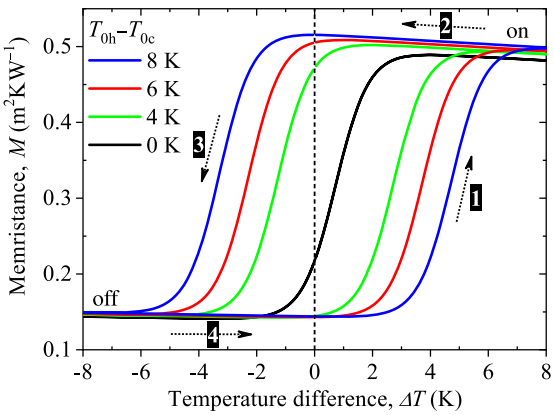

FIG. 5. Closed loops of the thermal memristance associated with the Lissajous curves shown in Fig. 4. Regimes 1, 2, 3, and 4 correspond to the four characteristic time zones highlighted in Fig. 3.

conductance of the system, and its value $[G(2) \approx 4\sigma\varepsilon_m T_0^3]$ for case 2 is smaller than the one $[G(4) \approx 4\sigma\varepsilon_i T_0^3]$ for case 4 because of $\varepsilon_m < \varepsilon_i$. The nonlinear behavior in cases 1 and 3 is due to the VO_2 phase transitions driving the emissivity variations displayed in Fig. 3. The absence of these changes near the extreme values (± 8 K) of ΔT induces the pinched shape of the Lissajous curve. Note that the amplitude (the differences between curves 1 and 2 and curves 3 and 4) of this defining curve of the thermal memristor is driven by the hysteresis ($T_{0h}-T_{0c} = 8$ K) of the VO_2 emissivity such that it disappears for $T_{0h}-T_{0c} = 0$ K, as shown in the inset of Fig. 4. This amplitude also increases with the emissivity contrast $\varepsilon_i/\varepsilon_m$ of VO_2, as shown in Fig. S2 of the Supplemental Material [51]. These facts make evident that the existence of the Lissajous $q-\Delta T$ curve is determined by the combined impact of the thermal hysteresis ($T_{0h} \neq T_{0c}$) and emissivity contrast ($\varepsilon_i/\varepsilon_m \neq 1$) of the involved PCM. This is confirmed by the areas of loops 1 and 2 and loops 3 and 4, which are equal and proportional to $(\varepsilon_i - \varepsilon_m)\sinh[\beta(T_{0h}-T_{0c})/2]$, as shown in the Supplemental Material [51]. This latter relation establishes the material requirements to optimize the performance and applications of the proposed thermal memristor.

Figure 5 shows the thermal memristances M related to the Lissajous $q-\Delta T$ curves displayed in Fig. 4 as functions of the temperature difference ΔT. The linear portions of the top (2) and bottom (4) lines correspond to the regimes without a phase transition of VO_2, while the complementary right (1) and left (3) lines result from its phase changes, in agreement with Figs. 3 and 4. The height of the $M-\Delta T$ loops is determined by the VO_2 emissivity contrast $\varepsilon_i/\varepsilon_m = 3.6$, which defines the on-off states of the memristance (Fig. 5) and is higher than that (1.6) of a conductive memristor [36]. The width of the memristance loop increases with the hysteresis $T_{0h}-T_{0c} > 0$ such that it disappears for $T_{0h}-T_{0c} = 0$, in agreement with Fig. 4.

In addition, the closed $M-\Delta T$ loops are similar to those of the electrical memristance [32], which indicates that what is done with electrical currents through the electrical memristor could also be done with thermal currents, by means of the thermal memristor. For instance, the thermal memristor could be used as a binary memory, in which the on and off values of the memristance (Fig. 5) are chosen to code the binary states 0 and 1, as is done with its electrical counterpart [32]. In addition, given that the proposed radiative memristor can be scaled down to nanometric dimensions through near-field radiation, this device has great potential for developing thermal memories that could complement the electronic flash ones.

Finally, we point out that, although the Lissajous $q-\Delta T$ curve reported in this Letter has been obtained with one PCM, we anticipate that this memristor effect can also be achieved with more complex systems involving a non-PCM with oscillating temperature [51] or two PCMs with temperatures properly modulated in time with equal or different frequencies. Furthermore, the development of the radiative memristor in the near field would allow not only its miniaturization but also the modulation of its memristance with the separation distance and steady-state temperature component T_0 of its terminals due to the strong dependence of the heat flux on these two parameters [52]. Radiative thermal memristors could thus be useful to tailor the heat transfer at different spatial scales.

In summary, the proof of principle of a radiative thermal memristor has been demonstrated by exploiting the thermal hysteresis of the emissivity of a phase change material exchanging radiative heat with a phase invariable one. For the case of VO_2, it has been shown that the Lissajous $q-\Delta T$ curve of the memristor yields a memristance whose temperature variations in a closed loop are determined by the hysteresis width of VO_2 and the ratio of emissivities for its insulating and metallic phases. Considering the unique thermal properties of the proposed thermal memristor, the

obtained results could open new research avenues in the development of thermal neurons, energy storage, and thermal management.

*jose.ordonez@cnrs.pprime.fr
†younes.ezzahri@univ-poitiers.fr

[1] B. Li, J. Lan, and L. Wang, Phys. Rev. Lett. **95**, 104302 (2005).
[2] B. Hu, L. Yang, and Y. Zhang, Phys. Rev. Lett. **97**, 124302 (2006).
[3] N. Yang, N. Li, L. Wang, and B. Li, Phys. Rev. B **76**, 020301(R) (2007).
[4] L. Wang and B. Li, Phys. World **21**, 27 (2008).
[5] J. Hu, X. Ruan, and Y. P. Chen, Nano Lett. **9**, 2730 (2009).
[6] N. Yang, G. Zhang, and B. Li, Appl. Phys. Lett. **95**, 033107 (2009).
[7] T. Ruokola, T. Ojanen, and A.-P. Jauho, Phys. Rev. B **79**, 144306 (2009).
[8] C. R. Otey, W. T. Lau, and S. Fan, Phys. Rev. Lett. **104**, 154301 (2010).
[9] S. Basu and M. Francoeur, Appl. Phys. Lett. **98**, 113106 (2011).
[10] H. Iizuka and S. Fan, J. Appl. Phys. **112**, 024304 (2012).
[11] L. Zhu, C. R. Otey, and S. Fan, Appl. Phys. Lett. **100**, 044104 (2012).
[12] Y. Yang, S. Basu, and L. Wang, Appl. Phys. Lett. **103**, 163101 (2013).
[13] B. Li, L. Wang, and G. Casati, Phys. Rev. Lett. **93**, 184301 (2004).
[14] M. Terraneo, M. Peyrard, and G. Casati, Phys. Rev. Lett. **88**, 094302 (2002).
[15] D. Segal, Phys. Rev. Lett. **100**, 105901 (2008).
[16] P. Ben-Abdallah and S.-A. Biehs, Appl. Phys. Lett. **103**, 191907 (2013).
[17] E. Nefzaoui, J. Drevillon, Y. Ezzahri, and K. Joulain, Appl. Opt. **53**, 3479 (2014).
[18] J. Ordonez-Miranda, J. M. Hill, K. Joulain, Y. Ezzahri, and J. Drevillon, J. Appl. Phys. **123**, 085102 (2018).
[19] J. Ordonez-Miranda, Y. Ezzahri, and K. Joulain, Phys. Rev. E **95**, 022128 (2017).
[20] B. Li, L. Wang, and G. Casati, Appl. Phys. Lett. **88**, 143501 (2006).
[21] H. Prod'homme, J. Ordonez-Miranda, Y. Ezzahri, J. Drevillon, and K. Joulain, J. Appl. Phys. **119**, 194502 (2016).
[22] P. Ben-Abdallah and S.-A. Biehs, Phys. Rev. Lett. **112**, 044301 (2014).
[23] K. Joulain, J. Drevillon, Y. Ezzahri, and J. Ordonez-Miranda, Phys. Rev. Lett. **116**, 200601 (2016).
[24] I. Latella, O. Marconot, J. Sylvestre, L. G. Fréchette, and P. Ben-Abdallah, Phys. Rev. Applied **11**, 024004 (2019).
[25] K. Joulain, Y. Ezzahri, J. Drevillon, and P. Ben-Abdallah, Appl. Phys. Lett. **106**, 133505 (2015).
[26] J. Ordonez-Miranda, Y. Ezzahri, J. Drevillon, and K. Joulain, J. Appl. Phys. **119**, 203105 (2016).
[27] L. Wang and B. Li, Phys. Rev. Lett. **99**, 177208 (2007).
[28] V. Kubytskyi, S.-A. Biehs, and P. Ben-Abdallah, Phys. Rev. Lett. **113**, 074301 (2014).
[29] K. Ito, K. Nishikawa, H. Iizuka, and H. Toshiyoshi, Appl. Phys. Lett. **105**, 253503 (2014).
[30] A. Fiorino, D. Thompson, L. Zhu, R. Mittapally, S.-A. Biehs, O. Bezencenet, N. El-Bondry, S. Bansropun, P. Ben-Abdallah, E. Meyhofer, and P. Reddy, ACS Nano **12**, 5774 (2018).
[31] K. Ito, K. Nishikawa, and H. Iizuka, Appl. Phys. Lett. **108**, 053507 (2016).
[32] R. Tetzla, *Memristors and Memristive Systems* (Springer, New York, 2014).
[33] L. O. Chua, IEEE Trans. Circuit Theory **18**, 507 (1971).
[34] D. B. Strukov, G. S. Snider, D. R. Stewart, and R. S. Williams, Nature (London) **453**, 80 (2008).
[35] P. Ben-Abdallah, AIP Adv. **7**, 065002 (2017).
[36] F. Yang, M. P. Gordon, and J. J. Urban, J. Appl. Phys. **125**, 025109 (2019).
[37] J. Ordonez-Miranda, Y. Ezzahri, K. Joulain, J. Drevillon, and J. J. Alvarado-Gil, Phys. Rev. B **98**, 075144 (2018).
[38] A. S. Barker, H. W. Verleur, and H. J. Guggenheim, Phys. Rev. Lett. **17**, 1286 (1966).
[39] M. Rini, A. Cavalleri, R. W. Schoenlein, R. López, L. C. Feldman, R. F. Haglund, L. A. Boatner, and T. E. Haynes, Opt. Lett. **30**, 558 (2005).
[40] M. M. Qazilbash, M. Brehm, B.-G. Chae, P.-C. Ho, G. O. Andreev, B.-J. Kim, S. J. Yun, A. V. Balatsky, M. B. Maple, F. Keilmann, H.-T. Kim, and D. N. Basov, Science **318**, 1750 (2007).
[41] M. M. Qazilbash, M. Brehm, G. O. Andreev, A. Frenzel, P.-C. Ho, B.-G. Chae, B.-J. Kim, S. J. Yun, H.-T. Kim, A. V. Balatsky, O. G. Shpyrko, M. B. Maple, F. Keilmann, and D. N. Basov, Phys. Rev. B **79**, 075107 (2009).
[42] K. Joulain, Y. Ezzahri, J. Drevillon, B. Rousseau, and D. D. S. Meneses, Opt. Express **23**, A1388 (2015).
[43] J. Yoon, H. Kim, X. Chen, N. Tamura, B. S. Mun, C. Park, and H. Ju, ACS Appl. Mater. Interfaces **8**, 2280 (2016).
[44] M. F. Modest, *Radiative Heat Transfer* (Academic Press, New York, 2013).
[45] S. Lee, K. Hippalgaonkar, F. Yang, J. Hong, C. Ko, J. Suh, K. Liu, K. Wang, J. J. Urban, X. Zhang, C. Dames, S. A. Hartnoll, O. Delaire, and J. Wu, Science **355**, 371 (2017).
[46] J. A. Ramirez-Rincon, C. L. Gomez-Heredia, A. Corvisier, J. Ordonez-Miranda, T. Girardeau, F. Paumier, C. Champeaux, F. Dumas-Bouchiat, Y. Ezzahri, K. Joulain, O. Ares, and J. J. Alvarado-Gil, J. Appl. Phys. **124**, 195102 (2018).
[47] C. L. Gomez-Heredia, J. A. Ramirez-Rincon, J. Ordonez-Miranda, O. Ares, J. J. Alvarado-Gil, C. Champeaux, F. Dumas-Bouchiat, Y. Ezzahri, and K. Joulain, Sci. Rep. **8**, 8479 (2018).
[48] J. Ordonez-Miranda, Y. Ezzahri, J. Drevillon, and K. Joulain, Phys. Rev. Applied **6**, 054003 (2016).
[49] J. Bodzenta, J. B. Burak, M. Nowak, M. Pyka, M. Szaajko, and M. Tanasiewicz, Dent. Mater. **22**, 617 (2006).
[50] F. Cervantes-Alvarez, J. D. Macias, and J. J. Alvarado-Gil, J. Phys. D **51**, 065302 (2018).
[51] See Supplemental Material at http://link.aps.org/supplemental/10.1103/PhysRevLett.123.025901 for an auxiliary description of the heat flux and the corresponding thermal memristance.
[52] I. Latella, R. Messina, J. M. Rubi, and P. Ben-Abdallah, Phys. Rev. Lett. **121**, 023903 (2018).